PHYSICAL REVIEW D **91,** 054005 (2015)

Shear viscosity and phase diagram from Polyakov–Nambu–Jona-Lasinio model

Sanjay K. Ghosh,[*] Sibaji Raha,[†] Rajarshi Ray,[‡] Kinkar Saha,[§] and Sudipa Upadhaya[‖]

Center for Astroparticle Physics and Space Science, Block-EN, Sector-V, Salt Lake, Kolkata 700091, India and Department of Physics, Bose Institute, 93/1, A. P. C Road, Kolkata 700009, India

(Received 11 November 2014; published 3 March 2015)

We present a detailed study of the variation of shear viscosity η, with temperature and baryon chemical potential within the framework of the Polyakov–Nambu–Jona-Lasinio model. η is found to depend strongly on the spectral width of the quasiparticles present in the model. The variation of η across the phase diagram has distinctive features for different kinds of transitions. These variations have been used to study the possible location of the critical end point and are cross-checked with similar studies of variations of specific heat. Finally, using a parametrization of the freeze-out surface in heavy-ion collision experiments, the variation of the shear viscosity to entropy density ratio has also been discussed as a function of the center-of-mass energy of collisions.

DOI: 10.1103/PhysRevD.91.054005 PACS numbers: 12.38.Aw, 12.38.Mh, 12.39.-x

I. INTRODUCTION

The relativistic heavy-ion collision experiments provide us with the unique opportunity to understand the physics of strongly interacting matter expected to be present in the Universe after a few microseconds of the big bang and possibly present in the interior of neutron stars. In the experiments, two heavy ions colliding at relativistic energies are expected to form a fireball consisting of deconfined quarks and gluons, popularly known as the quark-gluon plasma (QGP). The search for the QGP has continued for almost the last 30 years using several generations of higher energy accelerators such as BEVALAC, AGS, SPS, RHIC, and LHC, while covering a large energy range of a few AGeV to a few ATeV. Various observables, such as J/Ψ suppression [1] and strangeness enhancement [2], had been proposed as signatures of such a state of matter. All such proposed signatures are based on the medium's properties, which differ substantially in hadronic and quark phases. The possibility of observing charmonium suppression, for example, was proposed on the basis of the properties of deconfinement and plasma screening [1], whereas strangeness enhancement was proposed on the basis of chiral symmetry restoration, which may be fully realized in the QGP but only partially in a hadron gas [2,3].

If the main interest lies in the identification of a new form of bulk matter, then it is essential to choose observables corresponding to unique collective properties of this matter. For example, radial, azimuthal, and longitudinal flow are some of the relevant observables in heavy-ion collisions [4]. In general, such observables may be obtained from azimuthal Fourier components [5] $v_n(y, p_T, N_p, h)$ of the triple differential inclusive distribution of hadrons which are selected based on their impact parameter range.

The observation of elliptic flow in noncentral heavy-ion collisions at the RHIC may be considered as the most important evidence for the hydrodynamical behavior of the QGP. Elliptic flow occurs when the plasma collectively responds to pressure gradients in the initial state. Hydrodynamic evolution converts the initial pressure gradients to velocity gradients in the final state. In a heavy-ion collision one cannot control the deformation of the initial state. Instead, the deformation of the plasma is determined by the shape of the overlapping region of the colliding nuclei. This shape is governed by the impact parameter b. The impact parameter can be measured on an event-by-event basis using the azimuthal dependence of the spectra of produced particles. Once the impact parameter direction is known, the particle distribution can be expanded in Fourier components of the azimuthal angle ϕ. The Fourier coefficients (v_2, v_4, etc.) carry information about the deformation of the final state. For example, a positive v_2 implies the preferential emission of particles in the short direction, i.e., the presence of elliptic flow. Since shear viscosity η is expected to oppose the elliptic flow (and reduce v_2), it is necessary to incorporate η in the analysis. Moreover, a dimensionless quantity η/s, where s is the entropy density, tells us about the actual behavior of the fluid. The ratio η/s is akin to the inverse of the Reynolds number.

In general, η for a system of quasiparticles is expected to vary as $\sim \epsilon t_{mft}$, where ϵ is the energy density and t_{mft} is the average mean free time. The entropy density varies as $s \sim k_B n$, where k_B is the Boltzmann constant and n the number density. Since $\frac{\epsilon}{n}$ is the average energy per particle, considering the uncertainty principle one would get a lower

[*] sanjay@jcbose.ac.in
[†] sibaji@jcbose.ac.in
[‡] rajarshi@jcbose.ac.in
[§] saha.k.09@gmail.com
[‖] sudipa.09@gmail.com

bound on the product of ϵ/n and t_{mft}. In other words one would get $\eta/s \geq \frac{\hbar}{k_B}$. For the strong coupling limit of superconformal QCD, Policastro *et al.* [6] found $\eta/s = \frac{\hbar}{4\pi k_B}$. On the other hand, Kovtun *et al.* [7] conjectured $\frac{\eta}{s} \geq \frac{\hbar}{4\pi k_B}$ to be the lower bound (popularly known as Kovtun-Son-Starinets bound or in short KSS bound) for a wide class of systems. Interestingly, such a finite but low value of η/s is found to be consistent with the analysis of RHIC data through hydrodynamical simulations [8,9].

Thus, heavy-ion experiments suggest the formation of a QGP with a behavior of near-perfect fluidity, i.e., very low viscosity. There are different $(2+1)$d [10–13] and $(3+1)$d [14,15] viscous hydrodynamic codes which are used to estimate QGP viscosity from the experimental data using the elliptic flow coefficient v_2. The initial spatial deformation of the fireball created in relativistic heavy-ion experiments is converted into final state momentum anisotropies through hydrodynamic simulations. Viscosity comes into play via the degradation of this conversion efficiency. As in experimental detections only the final state hadrons are tracked; the most efficient observable to be related to these studies is the charged hadron elliptic flow $v_2^{\rm ch}$. Therefore, the best description is provided with the amalgamation of the viscous hydrodynamic approach to the QGP phase and a microscopic description for the rescattering of the late hadronic stage. Such hybrid approaches include VISHNU [16], which incorporates the VISH2 + 1 [10,17] algorithm with the UrQMD cascade model [18], and the McGill code, which connects $(3+1)$d viscous hydrodynamics to UrQMD. The pioneering study in this regard was carried out by Luzum and Romatschke [12] using $(2+1)$d viscous hydrodynamics. One of the points of uncertainty in these studies is the initial condition. Different initial conditions like in MC-KLN or MC-Glauber lead to uncertainties in the values of $(\frac{\eta}{s})_{\rm QGP}$ by a factor of 2 to 2.5 [19]. A recent study carried out using MUSIC + UrQMD [20], with the IP-Glasma initial conditions [21], shows an excellent match to multiplicity and flow distributions at the RHIC and LHC. In fluid dynamical descriptions of the created fireball, the shear viscosity to entropy density ratio $\frac{\eta}{s}$ is usually taken to be temperature independent. Predictions made in order to explain the azimuthal anisotropies of the spectra, like the elliptic flow coefficient v_2, reveal very a small value for this $\frac{\eta}{s} \sim 0.1$ [11,12,22,23]. However, there are some works including the temperature dependence of $\frac{\eta}{s}$ [24] as well, where the authors have taken different parametrizations to get a thorough understanding of the effect on elliptic flow as well as higher harmonics. Lattice studies of transport coefficients of a gluon plasma have also been carried out [25,26] indicating an ideal fluid behavior of the QGP.

There are different techniques which can be used for the evaluation of η in strongly interacting systems, namely, the relaxation time approach [27], the Chapman-Enskog method [28], and the Green-Kubo formalism [29]. In the relaxation time approach (RTA), it is assumed that the collisional effects drive the perturbed distribution function close to the equilibrium one with a relaxation time of the order of the time required for particle collisions. On the other hand, the Chapman-Enskog approximation is based on the fact that on a slight shift of the distribution function from its equilibrium value, the former can be expressed in terms of hydrodynamical variables and their gradients. One advantage of the Chapman-Enskog (CE) method is that one can do a successive approximation to get results closer to the Kubo formalism. The Green-Kubo formalism relates linear transport coefficients to near-equilibrium correlations of dissipative fluxes and treats them as perturbations to local thermal equilibrium. A comparative study of the three different methods has been carried out by Wiranata and Prakash [30]. In the varied cases considered there, the Green-Kubo technique is found to be more reliable. In Ref. [31] it has been argued that while in the case of CE, the variational method may yield solutions with arbitrary accuracy depending on the order of approximation, the RTA has no control over its accuracy. The RTA result was found to differ from that obtained using the Green-Kubo formalism by a factor of 2. On the other hand, the CE method, already at first order, was found to display satisfactory agreement with the Green-Kubo results. Comparisons in the context of the nonrelativistic hard sphere can be found in classical literature [32], from which it is inferred that higher order approximations of the CE method approach the Green-Kubo one. Notwithstanding this fact the RTA method has often been used due to its simplicity. It has been used to evaluate η for two-flavor matter in the Nambu–Jona-Lasinio (NJL) model [33–35]. On the other hand, in Refs. [36–40], a combination of large-N_c expansion and Kubo formalism was used to calculate η in the NJL model. In the present work we have used the framework of the 2 + 1-flavored Polyakov–Nambu–Jona-Lasinio (PNJL) model to study the behavior of η at finite temperature and density. The variation of η with temperature and density is then used to discuss the location of the critical end point (CEP).

The present article is organized as follows. The outline of the formalism adopted for this work is given in Sec. II followed by a brief introduction to the PNJL model in Sec. III. In Sec. IV A, we look for the variational nature of η with T for different choices of the spectral width Γ. Further, we compute η as a function of quark chemical potential μ_q for three different choices of T, viz., one in the expected range of the first order phase transition, another in the crossover range, and finally the last one beyond the crossover region. We also discuss the variation of $\frac{\eta}{s}$ as a function of μ_q for a wide range of T. In Sec. IV B, variation of $\frac{\eta}{s}$ with T at various μ_q has been used to draw the phase diagram and identify the CEP region. The location of the CEP is further validated with the behavior of the specific heat C_V in Sec. IV C. In Sec. IV D, we calculate $\frac{\eta}{s}$ under

different experimental conditions considering the freeze-out parametrization. Finally, the results are summarized in Sec. V.

II. KUBO FORMALISM

Kubo formalism, as mentioned earlier, involves the spectral width of the degrees of freedom of the system involved. This is realized through the fact that the shear viscosity coefficient η is related to retarded correlators of the energy-momentum (EM) tensor. The energy-momentum tensor is defined as $T_{\mu\nu} = i\bar{\psi}\gamma_\mu\partial_\nu\psi - g_{\mu\nu}\mathcal{L}$, where $\mathcal{L}$ is the PNJL Lagrangian. The Kubo formula for shear viscosity gives [40]

$$\eta(\omega) = \frac{1}{15T}\int_0^\infty dt e^{i\omega t}\int d\vec{r}(T_{\mu\nu}(\vec{r},t), T^{\mu\nu}(0,0)), \quad (1)$$

where $T_{\mu\nu}$ is the (μ,ν) component of the EM tensor of quark matter. The Kubo formula can also be rewritten in terms of only one component of the EM tensor, viz.,

$$\eta(\omega) = \beta\int_0^\infty dt e^{i\omega t}\int d\vec{r}(T_{21}(\vec{r},t), T_{21}(0,0)). \quad (2)$$

The conversion factor 15 between the above two equations comes from the following identity

$$\int d^3x x_i^2 x_j^2 f(x^2) = \frac{1}{15}\int d^3x x^4 f(x^2). \quad (3)$$

Starting from Eq. (2) and neglecting the surface terms at infinity, we arrive at the following expression of η in terms of the retarded correlators:

$$\eta(\omega) = \frac{i}{\omega}[\Pi^R(\omega) - \Pi^R(0)], \quad (4)$$

where $\Pi^R(\omega)$ is the retarded correlator defined as

$$\Pi^R(\omega) = -i\int_0^\infty dt e^{i\omega t}\int d^3\vec{r}\langle[T_{21}(\vec{r},t), T_{21}(0)]\rangle \quad (5)$$

considering only one component of the energy-momentum tensor. The static shear viscosity is then given by

$$\eta = -\frac{d}{d\omega}\mathrm{Im}\Pi^R(\omega)|_{\omega=0}. \quad (6)$$

To calculate the retarded correlator, one can switch to the Matsubara formalism in the form of Eq. (11) of Ref. [40]. Now, if we apply large-N_c expansion and consider scalar and pseudoscalar interactions [i.e., the vertex function Γ incorporating $(\mathbb{1}, i\gamma_5)$], the interaction kernels can be organized into ring diagrams with n loops. However, by doing so, the correlator is not affected at all as the trace in the first ring vanishes [37]

$$T\sum_n\int\frac{d^3p}{(2\pi)^3}\mathrm{Tr}[\gamma_2 G_\beta(\vec{p},\omega_n)\Gamma G_\beta(\vec{p},\omega_n)] = 0, \quad (7)$$

where $G_\beta(\vec{p},\omega_n) = \frac{\not{p}+M}{\omega_n^2+\vec{p}^2+M^2}$ with $\omega_n = (2n+1)\pi T - i\mu + A_4$, A_4 being the temporal component of the Euclidean gauge field through which the Polyakov line is represented. Other higher order corrections to this group will be least effective simply because every increase in the rank will generate a suppression factor $\sim\frac{1}{N_c}$. Effectively, we can restrict ourselves to the simple one-loop diagram for the correlation function in Matsubara space which upon using the one-component form of the energy-momentum tensor in Eq. (5) becomes [36]

$$\Pi(\omega_n) = \frac{1}{\beta}\sum_l\int\frac{d^3p}{(2\pi)^3}p_x^2\mathrm{Tr}[\gamma_2 G(\vec{p},\omega_l+\omega_n)\gamma_2 G(\vec{p},\omega_l)]. \quad (8)$$

To evaluate the Matsubara frequency summation, we use the spectral representation of the full propagator as

$$G(\vec{p},\omega_l) = \int_{-\infty}^\infty\frac{d\epsilon}{2\pi}\frac{\rho(\vec{p},\epsilon)}{i\omega_l-\epsilon} \quad (9)$$

with the effect of the background Polyakov loop incorporated accordingly. Here, $\rho(\vec{p},\epsilon)$ is the spectral function. Substituting Eq. (9) in Eq. (8) and replacing the summation by contour integration, we can write the trace as

$$\begin{aligned} S &\equiv T\sum_l\mathrm{Tr}[\gamma_2 G(\vec{p},\omega_l+\omega_n)\gamma_2 G(\vec{p},\omega_l)] \\ &= -\int_C\frac{dz}{2\pi i}f_\Phi(z)\mathrm{Tr}[G(\vec{p},z)\gamma_2 G(\vec{p},z+i\omega_n)\gamma_2], \end{aligned} \quad (10)$$

where $f_\Phi(z)$ is the modified Fermi-Dirac distribution function in the presence of the background Polyakov-loop field Φ and its conjugate $\bar{\Phi}$. The effect of incorporating the background Polyakov loop can be fully absorbed into the modified Fermi-Dirac distribution function [41,42]. To realize this, one can use the elements of the diagonalized A_4 matrix [43]. Thus, the usual Fermi-Dirac distribution function is replaced by the modified one in the following manner

$$\begin{aligned} n_F(\epsilon) &= (1+e^{\beta\epsilon})^{-1} \\ &\to -\frac{1}{\beta}\sum_i\frac{\partial\ln(1+e^{-\beta\epsilon}e^{-i\beta(A_4)_{ii}})}{\partial\epsilon} \to f_\Phi(\epsilon). \end{aligned}$$

Now, the contour C can be divided into pieces in order to avoid the branch cuts on $z=\epsilon$ and $z=\epsilon-i\omega_n$. As the integrals along large circles vanish on extending the real axis to infinity, one is left with the four lines infinitesimally close enough to the branch cuts and hence

$$S = -\int_{-\infty}^{\infty}\frac{d\epsilon}{2\pi i}f_\Phi(\epsilon)\mathrm{Tr}[G(\epsilon+i\delta)\gamma_2 G(\epsilon+i\omega_n)\gamma_2 - G(\epsilon-i\delta)\gamma_2 G(\epsilon+i\omega_n)\gamma_2 + G(\epsilon-i\omega_n)\gamma_2 G(\epsilon+i\delta)\gamma_2 - G(\epsilon-i\omega_n)\gamma_2 G(\epsilon-i\delta)\gamma_2], \quad (11)$$

where δ is an infinitesimally small positive number. Using the relation $G(\epsilon+i\delta)-G(\epsilon-i\delta)=-i\rho(\epsilon)$ and applying the analytic continuation $i\omega_n \to \omega + i\delta$, we can extract the imaginary part of S to be used in Eq. (6) [38]

$$\mathrm{Im}S = \int_{-\infty}^{\infty}\frac{d\epsilon}{2\pi}\frac{1}{2}f_\Phi(1-f_\Phi)\mathrm{Tr}[\rho(\epsilon+\omega)\gamma_2\rho(\epsilon)\gamma_2] \quad (12)$$

and hence

$$\eta = \frac{\pi}{T}\int_{-\infty}^{\infty}d\varepsilon\int\frac{d^3p}{(2\pi)^3}p_x^2 f_\Phi(1-f_\Phi)\mathrm{Tr}[\gamma_2\rho(\epsilon,p)\gamma_2\rho(\epsilon,p)]. \quad (13)$$

Using the standard form of the spectral function in terms of the advanced and retarded Green's function [36,40] we evaluate the trace to finally arrive at

$$\eta[\Gamma(p)] = \frac{16N_cN_f}{15\pi^3T}\int_{-\infty}^{\infty}d\varepsilon\int_0^{\infty}dp\,p^6\frac{M^2\Gamma^2(p)f_\Phi(\varepsilon)(1-f_\Phi(\varepsilon))}{((\varepsilon^2-p^2-M^2+\Gamma^2(p))^2+4M^2\Gamma^2(p))^2}, \quad (14)$$

where N_c and N_f are the number of colors and flavors, respectively. This is the expression for shear viscosity to be applied for this work. In the conventional notation, Γ(p) and M are the spectral width and the quasiparticle mass, respectively, coming through the definition of Green's functions. In the present context the thermal constituent quark mass M is modified with the eight-quark interaction term being incorporated into the PNJL Lagrangian as [44]

$$M = m_0 - 2g_S\sigma_f + \frac{g_D}{2}\sigma_{f+1}\sigma_{f+2} - 2g_1\sigma_f(\sigma_u^2+\sigma_d^2+\sigma_s^2) - 4g_2\sigma_f^3$$

with g_S and g_D being the four-quark and six-quark interaction couplings, respectively, whereas g_1 and g_2 refer to the eight-quark coupling. $\sigma_f = \langle\bar{\psi}_f\psi_f\rangle$ is the chiral condensate. If one considers $\sigma_f = \sigma_u$, then $\sigma_{f+1} = \sigma_d$ and $\sigma_{f+2} = \sigma_s$ or in cyclic order.

III. PNJL MODEL

The PNJL model [45–49] is a QCD-inspired phenomenological model developed by coupling the Polyakov-loop potential to the NJL model. In the NJL model, the interactions between quarks are accounted for by multi-quark terms which respect the global symmetries of QCD. Spontaneous breaking of chiral symmetry takes place due to the dynamical generation of fermion mass. Since the only effects of gluons come in effectively through the multiquark interactions, the NJL model fails to simulate various important facets of strong interactions. On the other hand some more features of the gluon physics are introduced into the PNJL in terms of the dynamics of a background field corresponding to the Polyakov loop. This helps in studying the important dynamics of chiral and deconfinement physics in an unified framework. Also, the thermodynamic properties in terms of pressure, entropy, conserved charge densities, and their fluctuations, etc., give more reliable estimates *vis-à-vis* lattice QCD results [49–51]. In the present work we have considered the $SU(3)_f$ version of the PNJL model including an eight-quark interaction [44]. The current quark masses used here are $m_u = m_d = 8.7$ MeV and $m_s = 179.5$ MeV along with the three momentum cutoff $\Lambda = 640$ MeV [44].

While computing the shear viscosity η as in Eq. (14), we incorporated the modified Fermi-Dirac distribution functions (f_Φ) in which the effect of the background Polyakov-loop fields is taken into account. The forms of the distribution functions for the particles and antiparticles as realized in the PNJL model are

$$f_\Phi^+(E_p) = \frac{(\bar{\Phi}+2\Phi e^{-\beta(E_p+\mu)})e^{-\beta(E_p+\mu)}+e^{-3\beta(E_p+\mu)}}{1+3(\bar{\Phi}+\Phi e^{-\beta(E_p+\mu)})e^{-\beta(E_p+\mu)}+e^{-3\beta(E_p+\mu)}}, \quad (15)$$

$$f_\Phi^-(E_p) = \frac{(\Phi+2\bar{\Phi}e^{-\beta(E_p-\mu)})e^{-\beta(E_p-\mu)}+e^{-3\beta(E_p-\mu)}}{1+3(\Phi+\bar{\Phi}e^{-\beta(E_p-\mu)})e^{-\beta(E_p-\mu)}+e^{-3\beta(E_p-\mu)}}, \quad (16)$$

where "±" refer to the particle and antiparticle, respectively. Φ and $\bar{\Phi}$ are the Polyakov-loop fields, μ and β being the chemical potential and inverse temperature, respectively. Starting from the PNJL thermodynamic potential we can calculate the fields (degrees of freedom of the system involved), pressure, and constituent masses at corresponding temperatures and chemical potentials. The details of the technique for two- and $2+1$-flavor cases can be found in Refs. [48,49] and Refs. [44,52], respectively. With these inputs, we proceed to determine η and s.

IV. RESULTS

A. Parametrization of Γ

The spectral width $\Gamma(\mathrm{p})$, in the PNJL model, is supposed to have contributions from the Landau damping of quarks and mesons along with the recombination processes, i.e., the formation of collective mesonic modes due to quark-antiquark rescattering. The spectral width for the two-flavor case including both σ and π has been evaluated at next-to-leading order in the large-N_c expansion including one-loop mesonic contributions [40,53]. Spectral widths evaluated this way would depend on both T and μ. In the case of the $SU(3)_f$ PNJL model all the scalar and pseudoscalar meson channels will contribute to this process. Moreover, the decay widths themselves may become comparable to or larger than the mass, especially at lower temperatures. Under such circumstances, one should really express η explicitly in terms of spectral functions which should then be evaluated considering all possible channels [54]. Since such a calculation is extremely involved, in our present work, we have considered the forms of $\Gamma(p)$ as given in Ref. [40]. The configurations of Γ proposed to ensure the convergence of η are

$$\begin{aligned}
\text{Constant:}\ \Gamma_{\text{const}} &= 100\ \text{MeV},\\
\text{Exponential:}\ \Gamma_{\text{exp}} &= \Gamma_{\text{const}} e^{-\beta p/8},\\
\text{Lorentzian:}\ \Gamma_{\text{Lor}}(p) &= \Gamma_{\text{const}} \frac{\beta p}{1+(\beta p)^2},\\
\text{Divergent:}\ \Gamma_{\text{div}}(p) &= \Gamma_{\text{const}} \sqrt{\beta p}.
\end{aligned}$$

Γ may also have some implicit dependence on N_f which is whatsoever not considered in the present work. The authors of Ref. [40] have calculated an effective spectral width at the one-loop level considering pseudoscalar and scalar channels under the two-flavor NJL model. There, the individual spectral widths for the scalar as well as the pseudoscalar channels are weighted by corresponding multiplicities. Such flavor dependence of the spectral width can be considered once Γ is obtained under the framework of the PNJL model and will be addressed in the future.

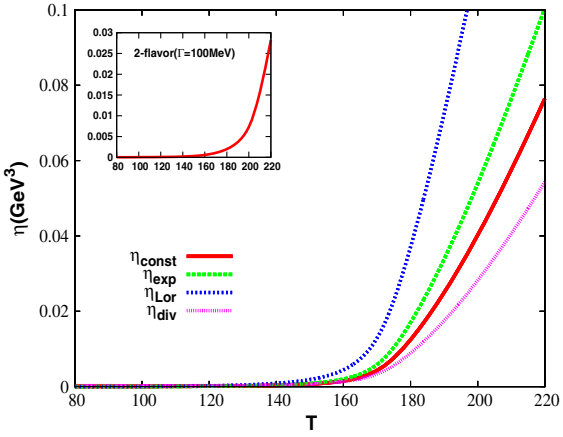

FIG. 1 (color online). η as a function of temperature at the vanishing chemical potential for different forms of Γ.

Figure 1 shows the variation of η with T, at $\mu_q = 0$, for different choices of Γ as given earlier, whereas in the inset, the result considering two flavors for a constant $\Gamma = 100$ MeV is shown with the parameter set adopted from Refs. [50,51]. For a given Γ, η is found to increase with temperature. This behavior is similar to a gaseous system where viscosity increases with temperature due to the increase in the average momentum of the particles [55]. In the present case, the sudden increase in η for $T \geq 160$ MeV may be attributed to the decrease in the constituent quark mass to the current quark mass. In the low temperature region, because of the large constituent quark masses, η is expected to fall as M^{-6}. It can also be seen that $\eta_{\text{Lor}} > \eta_{\text{exp}} > \eta_{\text{const}} > \eta_{\text{div}}$. This behavior simply depends on the value of Γ at a given temperature. A lower value of Γ corresponds to weaker interaction and hence a larger mean free path [40]. It is evident from Eq. (14) that the η for two-flavor matter will be less than the three-flavor matter for equal masses. Since the s quark mass is higher than the u and d masses, the difference is less than the equal mass case.

Variation of η with the quark chemical potential μ_q is shown in Fig. 2. Here, we have chosen three different temperatures $T = 100$, 150, and 200 MeV, corresponding to the first order phase transition and the crossover and beyond crossover regions. Similar to the zero chemical potential case, Fig. 2 also shows an increase in η with μ_q at fixed T. However, the nature of the curves is different for the three different choices of temperature. For $T = 100$ MeV, moving along the μ axis, one is expected to encounter the first order phase transition line. Here, η shows a jump for all forms of Γ at $\mu_q \simeq 280$ MeV. On the other hand, both for $T = 150$ MeV and $T = 200$ MeV Fig. 2 shows, as expected, a smooth variation in η along the μ_q direction.

It has already been mentioned that smaller Γ correspond to a larger η. Hence, the different forms of Γ, as observed earlier, only affect the rate at which η changes with T and μ_q. But these forms do not change the qualitative behavior of η, as seen from Figs. 1 and 2. As mentioned earlier, in an explicit calculation one should evaluate the spectral width $\Gamma(\mathrm{p})$ considering the contributions from all meson channels in the $SU(3)_f$ PNJL model. This $\Gamma(\mathrm{p})$ will depend on both T as well as μ_q. In the absence of such a rigorous evaluation, we would use the sum rule essential for the choice of the Breit-Wigner form, as a guiding principle [36,56],

$$\frac{1}{4}\mathrm{Tr}_{\text{spin}} \int_{-\infty}^{\infty} \frac{d\epsilon}{2\pi} [\rho(\epsilon, p)\gamma_0] = 1. \tag{17}$$

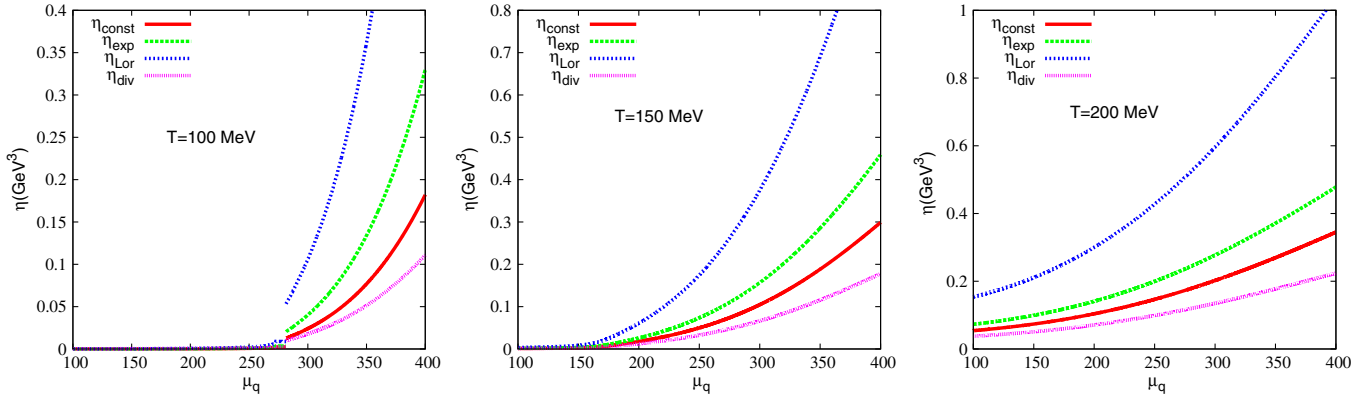

FIG. 2 (color online). η as a function of the quark chemical potential at fixed temperatures for different forms of Γ.

Equation (17) is satisfied approximately when the value of $\Gamma \leq M$. So, for our further discussions we choose a constant spectral width $\Gamma_{\text{const}} = 100$ MeV so that the sum rule is in general violated to a considerable extent only in the low momentum region. In fact, as the quark masses drop sharply around T_c, from its $T = \mu_q = 0$ value, the violation is expected to be more pronounced for $T > T_c$ only. But again the smaller contribution from low momentum at these high temperatures keeps the violation to a minimum level. For $\Gamma > 100$ MeV, the η variation is similar to that for Γ_{div}, whereas, for $\Gamma < 100$ MeV, it is similar to that for Γ_{Lor}. At the same time, in the regime of momentum transfer comparable to the QCD scale (~200 MeV), $\Gamma(p)$ becomes ~100 MeV considering contributions from one-loop mesonic channels at next-to-leading order in the large-N_c expansion as shown in Ref. [40]. There, the authors have included Landau damping and the recombination process as the leading dissipative effects to calculate shear viscosity at the one-loop level taking all mesons influencing the spectral width. However, going further up in the quark momentum leads towards a decrease in spectral width which in turn increases the shear viscosity.

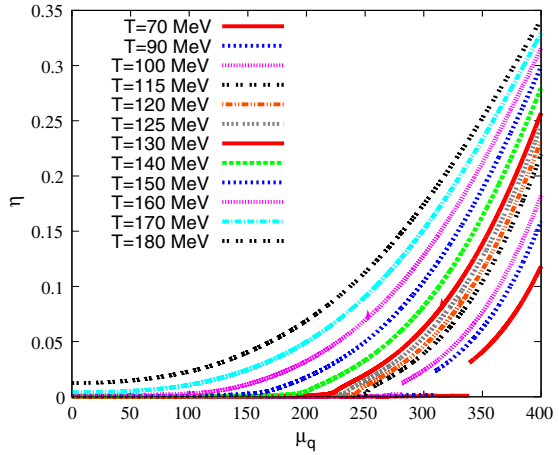

FIG. 3 (color online). Variation of shear viscosity with the quark chemical potential at different temperatures.

Let us again look at the variation of η with μ_q for different values of T with $\Gamma = 100$ MeV. From Fig. 3, two distinct regimes are clearly visible. For $T = 70$ to 100 MeV, we get a jump in η, whereas for $T = 120$ to 180 MeV, η has a smooth behavior analogous to the results displayed in Fig. 2. The temperature ranges $T = 70$–100 MeV and 120–180 MeV lie in the first order and crossover regions of the transition, respectively. The region around $T =$ 110–120 MeV calls for special attention and will be discussed in details below.

B. η/s and the phase diagram

In general, η for different fluids vary widely differing by orders of magnitude [55]. In such circumstances, the Reynolds number, the ratio of inertial to viscous forces in the Navier-Stokes equation, is traditionally used as a measure of fluidity. In the case of relativistic fluids, the Reynolds number (more specifically its inverse) may be defined in terms of η/s, s being the entropy density. Here, we present this ratio in Fig. 4 for $\mu_q = 0$ for the $2+1$-flavor quark matter in the PNJL model. We have shown

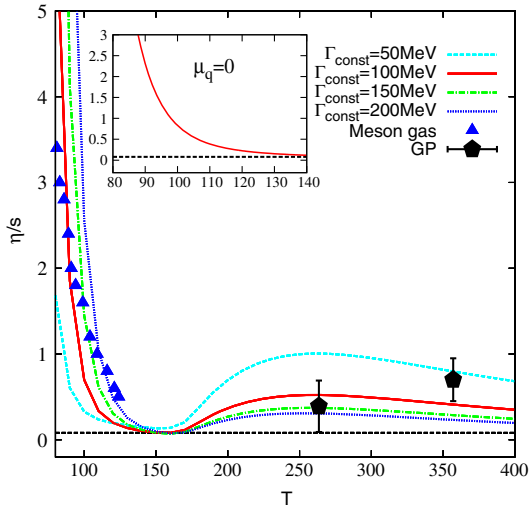

FIG. 4 (color online). Specific shear viscosity $(\frac{\eta}{s})$ as a function of temperature at the vanishing chemical potential.

comparative plots for different constant values of the spectral width to get a better understanding of the effect of Γ on the specific shear viscosity $\frac{\eta}{s}$.

As shown in Fig. 4 $\frac{\eta}{s}$ starts from high values at low temperatures and decreases to a minimum of $\frac{1}{4\pi}$ corresponding to ideal fluids near $T = T_c$. Though the η itself is extremely small for $T < T_c$, $\frac{\eta}{s}$ increases with decreasing temperature. The behavior of $\frac{\eta}{s}$ for this region of temperature is due to a larger drop in entropy density of the system. A simple calculation for pion gas shows $\frac{\eta}{s}$ to be proportional to $(\frac{f_\pi}{T})^4$ where f_π is the pion decay constant [57,58]. Hence, for T $\to$ 0, $\frac{\eta}{s}$ should diverge. Similar results have also been obtained by Lang *et al.* [59] who have computed $\frac{\eta}{s}$ for an interacting pion gas considering different pion masses. In the inset of Fig. 4, the region from $T = 80$ to 140 MeV has been zoomed in for a better comparison with the system of the interacting pion gas [59]. A comparison of our results in this temperature region with a corresponding result for meson gas ($T < T_c$) obtained from chiral perturbation theory [60] is also shown in Fig. 4.

In general, for an ideal gas of quarks, the η and hence $\frac{\eta}{s}$ should diverge at the large-T limit. As shown in Fig. 4 $\frac{\eta}{s}$ does show an increasing trend for $T > T_c$. The behavior of $\frac{\eta}{s}$ up to about $T \sim 1.5T_c$ seems to closely resemble the features of a fluid having a liquid-gas phase transition, for which a minimum is expected near the transition point [55,61]. However, since all the quark masses drop to their respective current masses for $T > 1.5T_c$, entropy starts dominating. As a result $\frac{\eta}{s}$ starts decreasing slowly with increasing T and hence displays a behavior of an interacting liquid. In lattice studies a similar behavior has been observed for pure glue plasma (GP) as shown in Fig. 4. The results of perturbation theory [62,63] are around 1 as both η and s vary as T^3 at higher temperatures. Eventually, for asymptotic temperatures an ideal gas behavior is expected to be restored. Near the phase transition region, the specific shear viscosity comes down to reach the KSS bound. This would then explain the results from the flow measurements in heavy-ion collision experiments if the system freeze-out occurs close to the transition. This reflects an important observation regarding the advantage of using PNJL over NJL. Though the behavior of $\frac{\eta}{s}$ in the PNJL model is qualitatively similar to those obtained in the NJL model [33,37,40], the modification of the quark distribution function, as well as the contribution to the entropy from the Polyakov loop, is vital in determining the quantitative results.

Similar features are observed with the increase in μ_q as shown in Fig. 5. To summarize the situation we see that $\frac{\eta}{s}$ initially decreases with an increase in T and reaches a minimum near the transition for the corresponding μ_q. Thereafter, it increases with T rather slowly after the transition before stabilizing/slowly decreasing in accordance with the behavior found in Refs. [25,26,64]. The minimum occurs close to the KSS bound as for $\mu_q \sim 100$–150 MeV. On the other hand, for $\mu_q \geq 200$ MeV, the system undergoes a transition at lower temperatures and $\frac{\eta}{s}$ has a minimum shifting upward from the KSS bound. Moreover, for $\mu_q \geq 260$ MeV, $\frac{\eta}{s}$ shows a jump which may be attributed to a first order phase transition. Therefore, a possibility of observing a CEP arises near these ranges of T and μ_q.

The critical end point bears special significance in the QCD phase diagram, where transport coefficients exhibit critical behavior. In Ref. [65], the authors have analyzed the dynamics near the critical point by constructing the Langevin equation near it and applying the dynamic renormalization group. It is seen that bulk viscosity and thermal conductivity strongly diverge and can be more important than shear viscosity near the QCD critical point. Another work using the same approach has been done in the framework of the O(N) scalar field theory [66] where the authors investigated the critical dynamics to determine the critical exponents of transport coefficients. The shear viscosity is found to remain finite for both single- and multicomponent theories in comparison to bulk viscosity which diverges for single-component theory. However, in this work we focus on locating the critical region in terms of changes in the behavioral pattern of the shear viscosity.

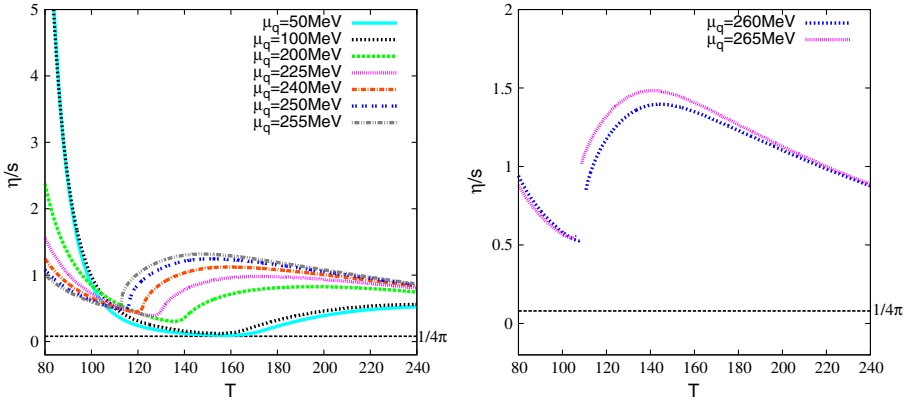

FIG. 5 (color online). $\frac{\eta}{s}$ as a function of temperature for different nonzero values of the quark chemical potential.

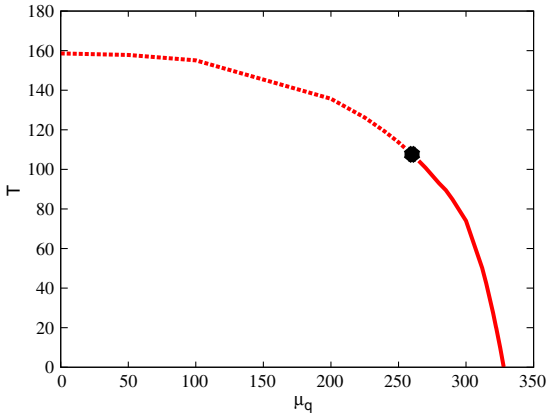

FIG. 6 (color online). Phase diagram for the 2 + 1-flavor PNJL model.

The QCD critical end point is supposed to be described by model H [67]. η is expected to diverge, with a small power of correlation length, near the CEP [68,69]. On the other hand, for weakly coupled real scalar field theories, $\frac{\eta}{s}$ is most likely to develop a cusp at the CEP [70]. A discontinuity in the behavioral pattern of $\frac{\eta}{s}$ around the CEP region has also been discussed in Ref. [33] using the NJL model.

In our study the location of the minima and the discontinuities of $\frac{\eta}{s}$ in Fig. 5 enable us to extract the critical values of T and μ to draw the phase diagram. However, in the very low temperature region extrapolation has been done considering the fitting function in the form of the polynomial

$$T = a_0 + a_1\mu + a_2\mu^2 \tag{18}$$

with $a_0 = 50$ MeV, $a_1 = -2.5$, and $a_2 = -0.04$ MeV^{-1}. The phase diagram along with the CEP region (black dot) has been plotted in Fig. 6.

C. On the location of the CEP

The understanding of the behavior of the strongly interacting system near the CEP along with its location is extremely important. Various efforts are being undertaken, both theoretically as well as experimentally, to determine the position of the CEP [64,71]. In general, second order derivatives of thermodynamic quantities are expected to diverge near the CEP which is a second order transition point. These quantities may provide additional information regarding the CEP. Here, in the PNJL model, we have observed that at or around the CEP, wide variations in order parameters, fluctuations of conserved charges like net electric charge [72], can occur as far as dynamic as well as static properties of the system are concerned.

In order to cross-check the location of the CEP obtained from the behavior of η/s, we have estimated the specific heat C_V, which is expected to show diverging behavior near the CEP. One can define C_V as

$$C_V = \frac{\partial\epsilon}{\partial T} = T\frac{\partial^2 P}{\partial T^2} = T\frac{\partial s}{\partial T}. \tag{19}$$

The divergence in C_V near the CEP will translate into highly enhanced transverse momentum fluctuations or highly suppressed temperature fluctuations for a system passing close to the CEP. In Fig. 7, we have shown the variation of the dimensionless quantity $\frac{C_V}{T^3}$ with T separately in the regions of crossover, the CEP, first order and beyond, along the μ_q direction. As is seen $\frac{C_V}{T^3}$ has a divergent behavior at around $T = 100$ MeV and $\mu_q \sim 260$ MeV but shows continuous behavior or at most a sharp peak elsewhere. Thus, we confirm that the CEP is expected to exist around $T = 100$–120 MeV and $\mu_q = 250$–270 MeV as inferred from the behavior of $\frac{\eta}{s}$ in the previous subsection.

D. Connection with experiments

In experiments, the observables are studied as a function of the center-of-mass collision energy ($\sqrt{s}$). In our thermodynamic studies the independent variables are T, the baryon chemical potential μ_B, the electric charge chemical potential μ_Q, and the strangeness chemical potential μ_S. So, to get the collision energy dependence one needs to get a

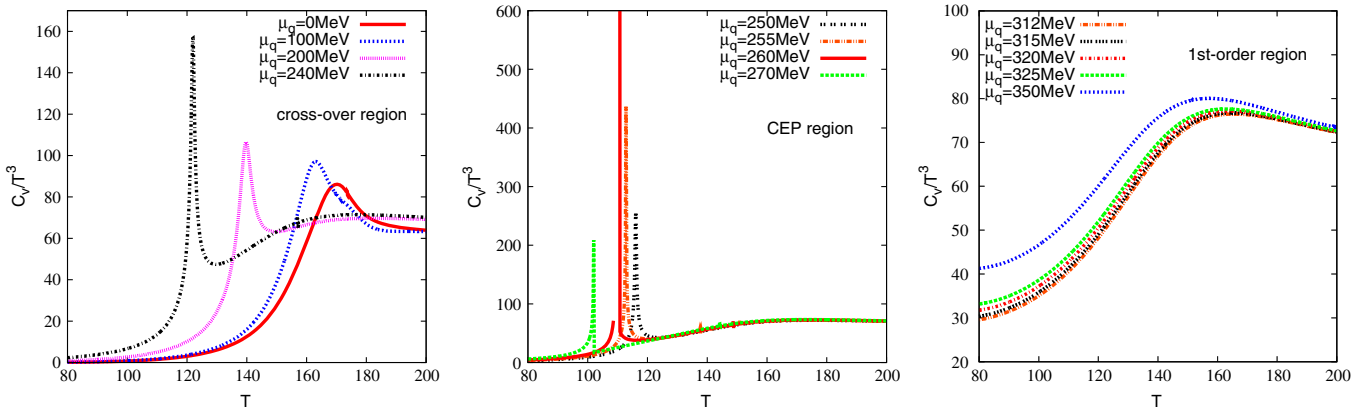

FIG. 7 (color online). C_V/T^3 as a function of temperature for different values of μ_q.

TABLE I. Parameters for extraction of chemical potentials along the freezeout curve.

	d[GeV]	e[GeV^{-1}]
B	1.308(28)	0.273(8)
Q	0.0211	0.106
S	0.214	0.161

parametrization of $\sqrt{s}$ with the various thermodynamic variables at freeze-out. Different parametrizations of the freeze-out conditions as a function of $\sqrt{s}$ are available in the literature [73,74]. For a given set of the thermodynamic variables, the variations in $\sqrt{s}$ are within 10% for different parametrizations. In the present study we have used the following parametrization [73]:

$$T^f(\mu_B^f) = a - b\mu_B^{f\,2} - c\mu_B^{f\,4} \quad \text{with } \mu_{B,Q,S}^f(\sqrt{s}) = \frac{d}{1 + e\sqrt{s}}, \tag{20}$$

where the superscript f denotes values at freeze-out, $a = (0.166 \pm 0.002)$ GeV, $b = (0.139 \pm 0.016)$ GeV^{-1}, $c = (0.053 \pm 0.021)$ GeV^{-3}, and d and e are given by Table I.

The variation of $\frac{\eta}{s}$ as a function of $\sqrt{s}$ at the freeze-out is displayed in Fig. 8. We have plotted the specific shear viscosity considering a spectral width of 100 and 200 MeV. We have already seen that an increase in Γ results in the decrease in η. This is true for the nonvanishing chemical potential as well. It can be seen that $\frac{\eta}{s}$ saturates to the KSS bound for $\Gamma = 200$ MeV whereas for $\Gamma = 100$ MeV saturation occurs at higher values. Therefore, as expected a stronger interaction (in terms of Γ) seems to be necessary to attain the KSS bound.

At the RHIC, the large azimuthal anisotropy of transverse momentum (p_T) spectra, often expressed by the elliptic flow coefficient v_2, has been observed and this is considered to be a signature for the formation of the QGP.

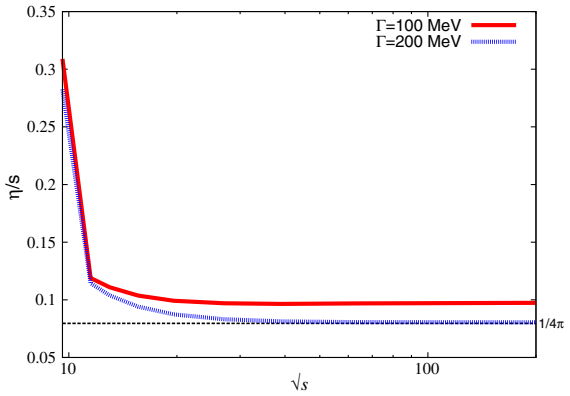

FIG. 8 (color online). $\frac{\eta}{s}$ under different center-of-mass energies at freeze-out.

The observed transverse momentum spectra of the hadrons and their centrality dependence [8,21–24,75] in relativistic heavy-ion collision experiments can be explained satisfactorily using fluid dynamic descriptions. In fact, the notion of small $\frac{\eta}{s}$ for the QGP arose from analysis of the RHIC data through hydrodynamical simulations [9,11,19,23,75] which indicate nonviscous fluid properties for the QGP. Though there have been predictions from various hydrodynamic calculations and simulations regarding temperature-independent η, uncertainties occur because of different initial conditions used. For example, use of data from Au + Au collisions at the RHIC leads to $(\frac{\eta}{s})_{\rm QGP} \sim 0.08$ with MC-Glauber initializations, whereas that with MC-KLN results in 0.16 [19]. Moreover, analysis at LHC energies for Pb + Pb collisions provides a bit higher result ~0.2 with various parametrizations incorporating different initial conditions [24,76].

Our results as shown in Fig. 8 are close to $\frac{\eta}{s} \sim 0.09 \pm 0.015$ [64,77] as extracted from the RHIC data for Au + Au collisions. Gavin and Abdel-Aziz [78] estimated, from the STAR data analysis, $\frac{\eta}{s}$ to lie in the range of 0.08–0.3. Another estimate done for the top RHIC energies renders a value of $\frac{\eta}{s} = 0.12$ [76] which is also close to our model results.

However, it should be noted that the results presented here are those of a system that has frozen out at complete thermodynamic equilibrium. Moreover, along the freeze-out curve, we always reside in the hadronic phase. So, the value of $\frac{\eta}{s}$ in Fig. 8 corresponds to different conditions in the hadronic sector. Initially, $\frac{\eta}{s}$ decreases with $\sqrt{s}$ and then saturates at a value close to the KSS bound for higher $\sqrt{s}$. This is a reflection of the variation of $\frac{\eta}{s}$ as shown in Figs. 4 and 5. Whether the signatures of crossover or the CEP survive the dynamics of fireball evolution cannot be addressed within the present formalism. A detailed hydrodynamical flow study incorporating both equilibrium and possible out-of-equilibrium features would be necessary to estimate such effects. Such signatures may show up in experimental analysis if the data points are found to be substantially higher than those in Fig. 8. Since the upcoming CBM experiments at the FAIR facility are going to look for the high density system for low $\sqrt{s}$ it would be interesting to look for such signatures of the CEP there.

V. CONCLUSION

In the present study the PNJL model has been used to calculate shear viscosity η at finite temperature and chemical potential using the Kubo formalism. The effect of spectral width Γ has been discussed and finally constant Γ has been used to present the rest of our results. The behavior of $\frac{\eta}{s}$ with T and μ_q has been used to locate the CEP. This location of the CEP has also been cross-checked from the divergent behavior of specific heat C_V with T and μ_q. Finally, we have studied the variation of $\frac{\eta}{s}$ with $\sqrt{s}$ to

compare with the values extracted from the analysis of RHIC and LHC data existing in the literature.

The salient points of the present study are the following.

(i) η by itself seems to show a gaslike behavior and increases with increasing temperature. It has a strong dependence on the spectral width Γ, especially at higher temperatures.

(ii) At $\mu_q = 0$, $\frac{\eta}{s}$ in the PNJL model seems to reproduce the pion gas feature at low temperature and QGP features at high temperatures. Near T_c, $\frac{\eta}{s}$ has a minimum at the KSS bound. For $T > T_c$, $\frac{\eta}{s}$ initially increases and then starts decreasing with increasing temperature showing a liquidlike behavior.

(iii) The qualitative features in both the PNJL and NJL models are quite similar. However, the results are quantitatively quite different in the two models. The satisfactory quantitative agreement with hadron gas at low temperatures and QGP at high temperatures shows the necessity of introducing the Polyakov-loop effects to the NJL model.

(iv) For nonzero μ_q, the behavior of $\frac{\eta}{s}$ remains similar to that at $\mu_q = 0$. However, the minimum value of $\frac{\eta}{s}$ occurring at the respective crossover or transitions is found to increase for larger μ_q and does not reach the KSS bound for $\mu_q \geq 200$ MeV.

(v) Variation of η across the phase boundary depends strongly on the nature of the phase transition. In the crossover region, $\frac{\eta}{s}$ changes continuously with μ_q whereas it shows a jump in the first order transition region. The change in the nature of variation, in going from crossover to first order, may be used to extract the information of the CEP. According to the present analysis, the CEP seems to lie in the range $T = 100$–120 MeV and $\mu_q = 250$–270 MeV.

(vi) $\frac{\eta}{s}$ on the freeze-out curve seems to agree with the values extracted from the RHIC and LHC flow analysis. It would be interesting to see if signatures of the CEP may be captured at lower $\sqrt{s}$ in the upcoming CBM experiments at the FAIR facility.

It may be useful to discuss a flow analysis of the experimental data with the inclusion of T and μ_q dependence of $\frac{\eta}{s}$ as obtained here, which we hope to pursue in the future.

ACKNOWLEDGMENTS

The authors would like to thank CSIR and DST for funding this work. S. U. thanks Avik Banerjee for a few useful discussions regarding the framework of the Kubo formalism. S. U. and K. S. acknowledge Sabyasachi Ghosh and Sarbani Majumder for useful suggestions.

[1] T. Matsui and H. Satz, Phys. Lett. **178B**, 416 (1986).
[2] P. Koch, B. Müller, and J. Rafelski, Phys. Rep. **142**, 167 (1986).
[3] H. Meyer-Ortmanns, Rev. Mod. Phys. **68**, 473 (1996).
[4] H. Stocker, Nucl. Phys. **A750**, 121 (2005); P. Bozek and I. Wyskiel, Phys. Rev. C **81**, 054902 (2010); J. Steinheimer, J. Auvinen, H. Petersen, M. Bleicher, and H. Stöcker, Phys. Rev. C **89**, 054913 (2014).
[5] J. Y. Ollitrault, Phys. Rev. D **46**, 229 (1992).
[6] G. Policastro, D. T. Son, and A. O. Starinets, Phys. Rev. Lett. **87**, 081601 (2001).
[7] P. Kovtun, D. T. Son, and A. O. Starinets, Phys. Rev. Lett. **94**, 111601 (2005).
[8] P. Huovinen and P. V. Ruuskanen, Annu. Rev. Nucl. Part. Sci. **56**, 163 (2006).
[9] H. Niemi, G. S. Denicol, P. Huovinen, E. Molnár, and D. H. Rischke, Phys. Rev. Lett. **106**, 212302 (2011).
[10] H. Song and U. Heinz, Phys. Lett. B **658**, 279 (2008); Phys. Rev. C **77**, 064901 (2008).
[11] P. Romatschke and U. Romatschke, Phys. Rev. Lett. **99**, 172301 (2007).
[12] M. Luzum and P. Romatschke, Phys. Rev. C **78**, 034915 (2008).
[13] K. Dusling and D. Teaney, Phys. Rev. C **77**, 034905 (2008); P. Bozek, Phys. Rev. C **81**, 034909 (2010); A. K. Chaudhuri, J. Phys. G **37**, 075011 (2010).
[14] B. Schenke, S. Jeon, and C. Gale, Phys. Rev. Lett. **106**, 042301 (2011).
[15] P. Bozek, Phys. Rev. C **85**, 034901 (2012).
[16] H. Song, S. A. Bass, and U. Heinz, Phys. Rev. C **83**, 024912 (2011).
[17] C. Shen and U. Heinz, Phys. Rev. C **83**, 044909 (2011).
[18] S. A. Bass *et al.*, Prog. Part. Nucl. Phys. **41**, 255 (1998); M. Bleicher *et al.*, J. Phys. G **25**, 1859 (1999).
[19] U. Heinz and R. Snellings, Annu. Rev. Nucl. Part. Sci. **63**, 123 (2013).
[20] S. Ryu, S. Jeon, C. Gale, B. Schenke, and C. Young, Nucl. Phys. **904–905**, 389c (2013).
[21] B. Schenke, P. Tribedy, and R. Venugopalan, Phys. Rev. Lett. **108**, 252301 (2012); Phys. Rev. C **86**, 034908 (2012).
[22] H. Song, S. A. Bass, U. Heinz, T. Hirano, and C. Shen, Phys. Rev. C **83**, 054910 (2011).
[23] H. Song, S. A. Bass, U. Heinz, T. Hirano, and C. Shen, Phys. Rev. Lett. **106**, 192301 (2011).
[24] H. Niemi, G. S. Denicol, P. Huovinen, E. Molnar, and D. H. Rischke, Phys. Rev. C **86**, 014909 (2012).
[25] A. Nakamura and S. Sakai, Phys. Rev. Lett. **94**, 072305 (2005).
[26] H. B. Meyer, Phys. Rev. D **76**, 101701 (2007).
[27] P. Chakraborty and J. I. Kapusta, Phys. Rev. C **83**, 014906 (2011).

[28] W. A. van Leeuwen, P. Polak, and S. R. de Groot, Physica (Amsterdam) **63**, 65 (1973).
[29] R. Kubo and K. Tomita, J. Phys. Soc. Jpn. **9**, 888 (1954); H. Nakano, Prog. Theor. Phys. **15**, 77 (1956); R. Kubo, J. Phys. Soc. Jpn. **12**, 570 (1957).
[30] A. Wiranata and M. Prakash, Phys. Rev. C **85**, 054908 (2012).
[31] S. Plumari, A. Puglisi, F. Scardina, and V. Greco, Phys. Rev. C **86**, 054902 (2012).
[32] J. A. McLennan, *Introduction to Non-equilibrium Statistical Mechanics*, 1st ed. (Prentice-Hall, Englewood Cliffs, NJ, 1989).
[33] C. Sasaki and K. Redlich, Nucl. Phys. **A832**, 62 (2010).
[34] S. Ghosh, A. Lahiri, S. Majumder, R. Ray, and S. K. Ghosh, Phys. Rev. C **88**, 068201 (2013).
[35] R. Marty, E. Bratkovskaya, W. Cassing, J. Aichelin, and H. Berrehrah, Phys. Rev. C **88**, 045204 (2013).
[36] M. Iwasaki, H. Ohnishi, and T. Fukutome, arXiv:hep-ph/0606192v1.
[37] T. Fukutome and M. Iwasaki, Prog. Theor. Phys. **119**, 991 (2008).
[38] M. Iwasaki, H. Ohnishi, and T. Fukutome, J. Phys. G **35**, 035003 (2008).
[39] W.-j. Fu, Phys. Rev. D **88**, 036012 (2013).
[40] R. Lang and W. Weise, Eur. Phys. J. A **50**, 63 (2014).
[41] P. Deb, A. Bhattacharyya, S. Datta, and S. K. Ghosh, Phys. Rev. C **79**, 055208 (2009).
[42] C. A. Islam, S. Majumder, N. Haque, and M. G. Mustafa, J. High Energy Phys. 02 (2015) 011.
[43] H. Hansen, W. M. Alberico, A. Beraudo, A. Molinari, M. Nardi, and C. Ratti, Phys. Rev. D **75**, 065004 (2007).
[44] A. Bhattacharyya, P. Deb, S. K. Ghosh, and R. Ray, Phys. Rev. D **82**, 014021 (2010).
[45] P. N. Meisinger and M. C. Ogilvie, Phys. Lett. B **379**, 163 (1996); Nucl. Phys. B, Proc. Suppl. **47**, 519 (1996).
[46] K. Fukushima, Phys. Lett. B **591**, 277 (2004).
[47] E. Megias, E. R. Arriola, and L. L. Salcedo, Phys. Rev. D **74**, 065005 (2006); **74**, 114014 (2006); J. High Energy Phys. 01 (2006) 073.
[48] C. Ratti, M. A. Thaler, and W. Weise, Phys. Rev. D **73**, 014019 (2006).
[49] S. K. Ghosh, T. K. Mukherjee, M. G. Mustafa, and R. Ray, Phys. Rev. D **77**, 094024 (2008).
[50] S. K. Ghosh, T. K. Mukherjee, M. G. Mustafa, and R. Ray, Phys. Rev. D **73**, 114007 (2006).
[51] S. Mukherjee, M. G. Mustafa, and R. Ray, Phys. Rev. D **75**, 094015 (2007).
[52] M. Ciminale, R. Gatto, N. D. Ippolito, G. Nardulli, and M. Ruggieri, Phys. Rev. D **77**, 054023 (2008).
[53] D. Muller, M. Buballa, and J. Wambach, Phys. Rev. D **81**, 094022 (2010).
[54] P. Czerski, W. M. Alberico, S. Chiacchiera, A. De Pace, H. Hansen, A. Molinari, and M. Nardi, J. Phys. G **36**, 025008 (2009).
[55] T. Schafer and D. Teaney, Rep. Prog. Phys. **72**, 126001 (2009).
[56] W. M. Alberico, S. Chiacchiera, H. Hansen, A. Molinari, and M. Nardi, Eur. Phys. J. A **38**, 97 (2008).
[57] J. I. Kapusta, in *Relativistic Nuclear Collisions*, edited by R. Stock, Landolt-Bornstein New Series, Vol. I/23 (Springer-Verlag, Berlin, 2010).
[58] M. Prakash, M. Prakash, R. Venugopalan, and G. Welke, Phys. Rep. **227**, 321 (1993).
[59] R. Lang, N. Kaiser, and W. Weise, Eur. Phys. J. A **48**, 109 (2012).
[60] J. W. Chen and E. Nakano, Phys. Lett. B **647**, 371 (2007).
[61] J. Frenkel, *Kinetic Theory of Liquids* (Dover, New York, 1955); H. Eyring, J. Chem. Phys. **4**, 283 (1936); D. Tabor, *Gases, Liquids and Solids*, 2nd ed. (Cambridge University Press, Cambridge, England, 1979).
[62] P. Arnold, G. D. Moore, and L. G. Yaffe, J. High Energy Phys. 05 (2003) 051.
[63] J. P. Blaizot, E. Iancu, and A. Rebhan, Phys. Rev. Lett. **83**, 2906 (1999).
[64] R. A. Lacey, N. N. Ajitanand, J. M. Alexander, P. Chung, W. G. Holzmann, M. Issah, A. Taranenko, P. Danielewicz, and H. Stocker, Phys. Rev. Lett. **98**, 092301 (2007).
[65] Y. Minami, Phys. Rev. D **83**, 094019 (2011).
[66] E. Nakano, V. Skokov, and B. Friman, Phys. Rev. D **85**, 096007 (2012).
[67] D. T. Son and M. A. Stephanov, Phys. Rev. D **70**, 056001 (2004).
[68] P. C. Hohenberg and B. I. Halperin, Rev. Mod. Phys. **49**, 435 (1977).
[69] A. Onuki, Phys. Rev. E **55**, 403 (1997).
[70] J. W. Chen, M. Huang, Y. H. Li, E. Nakano, and D. L. Yang, Phys. Lett. B **670**, 18 (2008).
[71] R. A. Lacey, N. N. Ajitanand, J. M. Alexander, P. Chung, J. Jia, A. Taranenko, and P. Danielewicz, arXiv:0708.3512v6.
[72] A. Bhattacharyya, S. Das, S. K. Ghosh, S. Raha, R. Ray, K. Saha, and S. Upadhaya, arXiv:1212.6010v1.
[73] F. Karsch and K. Redlich, Phys. Lett. B **695**, 136 (2011).
[74] A. Andronic, P. Braun-Munzinger, and J. Stachel, Nucl. Phys. **A772**, 167 (2006).
[75] C. Shen, U. Heinz, P. Huovinen, and H. Song, Phys. Rev. C **82**, 054904 (2010).
[76] C. Gale, S. Jeon, B. Schenke, P. Tribedy, and R. Venugopalan, Phys. Rev. Lett. **110**, 012302 (2013).
[77] R. A. Lacey, Nucl. Phys. **A785**, 122 (2007).
[78] D. Teaney, Phys. Rev. C **68**, 034913 (2003); S. Gavin and M. Abdel-Aziz, Phys. Rev. Lett. **97**, 162302 (2006).